ACS OMEGA

http://pubs.acs.org/journal/acsodf

Article

Visualized and Quantitative Conformational Analysis of Peptidomimetics

Hajime Takashima,* Atsushi Yoshimori, Eiji Honda, Tomonori Taguri, Jun Ozawa, Masaji Kasai, Satoshi Shuto, and Dai Takehara

Cite This: *ACS Omega* 2021, 6, 26601−26612

Read Online

ACCESS | Metrics & More | Article Recommendations | Supporting Information

ABSTRACT: Protein−protein interactions (PPIs) are fundamentally important and challenging drug targets. Peptidomimetic molecules of various types have been developed to modulate PPIs. A particularly promising drug discovery strategy, structural peptidomimetics, was designed based on special mimicking of side-chain $C_\alpha-C_\beta$ bonds. It is simple and versatile. Nevertheless, no quantitative method has been established to evaluate its similarity to a target peptide motif. We developed two methods that enable visual, comprehensive, and quantitative analysis of peptidomimetics: peptide conformation distribution (PCD) plot and peptidomimetic analysis (PMA) map. These methods specifically examine multiple side-chain $C_\alpha-C_\beta$ bonds of a peptide fragment motif and their corresponding bonds (pseudo-$C_\alpha-C_\beta$ bonds) in a mimetic molecule instead of φ and ψ angles of a single amino acid in the traditional Ramachandran plot. The PCD plot is an alignment-free method, whereas the PMA map is an alignment-based method providing distinctive and complementary analysis. Results obtained from analysis using these two methods indicate our multifacial α-helix mimetic scaffold **12** as an excellent peptidomimetic that can precisely mimic the spatial positioning of side-chain functional groups of α-helix. These methods are useful for visualized and quantified evaluation of peptidomimetics and for the rational design of new mimetic scaffolds.

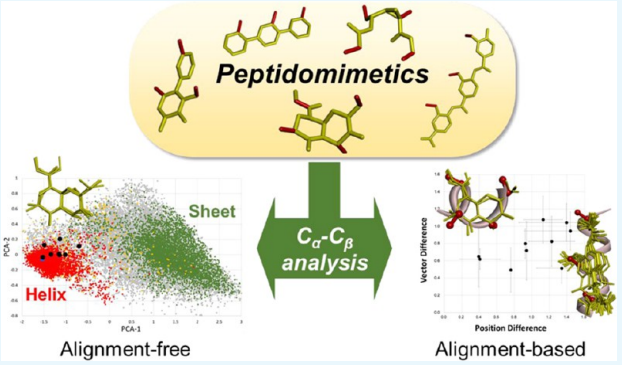

INTRODUCTION

Protein−protein interactions (PPIs) are involved in many regulatory pathways such as signal transduction, receptor−ligand interaction, cell metabolism, and transport across membranes. Often, PPIs are mediated by a "hot spot" amino acid side-chain functionality organized on secondary structures.[1−3] Modulation and inhibition of PPIs by peptidomimetics is a promising strategy for drug discovery.[4] The α-helix, which is the most common secondary structure on the surface of proteins, frequently mediates interactions of proteins with binding partners. In fact, 62% of PPIs in the Protein Data Bank (PDB) have an α-helix at the interface,[5] underscoring the importance of the secondary structure for protein−protein recognition. The mimetic of an α-helix structure is of considerable interest for drug discovery for PPI modulators.

Efforts to mimic an α-helix structure have led to several synthetic strategies such as helix stabilization, helical foldamers, side-chain mimetics, and pharmacophore mimetics on a helical surface. Grossmann et al.[6] introduced four distinctive classifications of peptidomimetics including α-helix mimetics: minor modified peptides/stapled peptides (Class A); major modified peptides/foldamers (Class B); structural mimetics (Class C); and mechanistic mimetics/pharmacophore mimetics (Class D). Classes A and B are modified peptide compounds. Classes C and D are completely nonpeptide small molecules. Among them, structural mimetics is a definite and versatile drug discovery strategy for providing fine α-helix mimetics because the scaffold of a mimetic molecule completely replaces the helical backbone. Key residues are also involved in the mimetics. The basic concept of Class C structural mimetics is that the side-chain $C_\alpha-C_\beta$ bond of a peptide fragment is projected to the bond of the side chain in structural mimetics. For this study, we defined the bond mimicking the side-chain $C_\alpha-C_\beta$ bond of a peptide fragment as the "pseudo-$C_\alpha-C_\beta$ bond" (Figure 1a, red stick). Arora et al.[7] reported that preferred side-chain rotamers of a peptide contribute directly to specificity in protein complex formation, indicating the importance of the $C_\alpha-C_\beta$ bond mimetics strategy. In contrast to Class C, the side-chain functional group constituting the pharmacophore of a peptide is involved as pharmacophore mimetics in Class D. The pharmacophore mimetics is connected to the mimetics core

Received: July 25, 2021
Accepted: September 14, 2021
Published: September 27, 2021

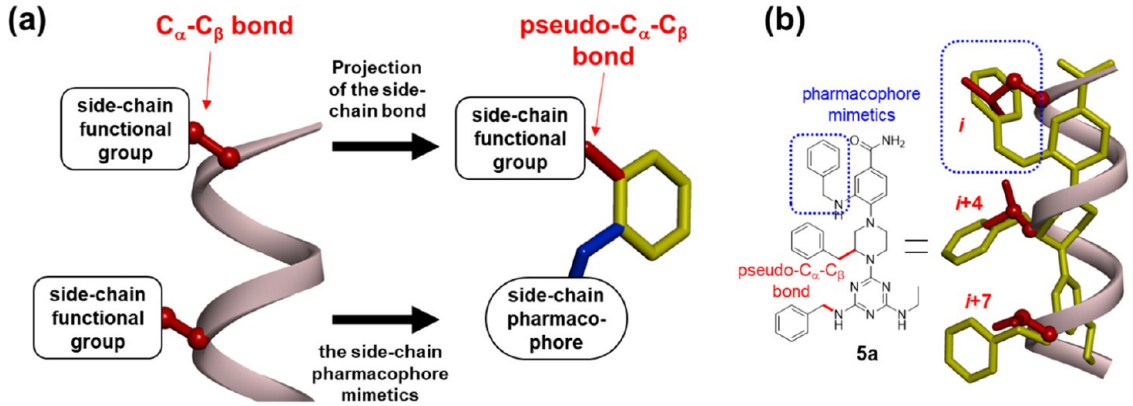

Figure 1. "Pseudo-C_α−C_β bond" and pharmacophore mimetics. (a) Pseudo-C_α−C_β bond (stick in red) is a bond of a mimetic molecule, which corresponds exactly to the side-chain C_α−C_β bond (ball-and-stick in red) of a peptide fragment (ribbon in pink). In pharmacophore mimetics, a side-chain pharmacophore is connected to a linkage (stick in blue) other than a pseudo-C_α−C_β bond. (b) Example of **5a**. The *i* side chain is pharmacophore mimetics, whereas the *i*+4 and *i*+7 side chains are pseudo-C_α−C_β bonds.

moiety by a linkage (Figure 1a, blue stick) other than a pseudo-C_α−C_β bond, i.e., a linkage that does not correspond to the C_α−C_β bond of a peptide fragment.

Many groups have reported structural peptidomimetics of various types with conformationally restricted scaffolds.[8−10] An α-helix displays and uses residues on one, two, or multiple faces for molecular recognition. Similarly, mimetic compounds are classified with single-facial, double-facial, and multifacial mimetics. In these mimetics, single-facial helix mimetics is the most well known and successful. Single-facial helix mimetics incorporates the *i*, *i*+4, and *i*+7 interacting side chains aligned on the same face of an α-helix (Figure 2a).[11−18] These mimetic molecules have exhibited binding and inhibitory activities for α-helix-related PPI targets, although most early studies have emphasized the examination of one-facial mimetics with hydrophobic residues. The pseudo-C_α−C_β bonds in these structural mimetics, shown in Figure 2, are assigned based on the mimetics design described in the original papers. It is noteworthy that scaffolds **1**,[11,12] **2**,[13] **3**,[14] and **4**[15] have three pseudo-C_α−C_β bonds (*i*, *i*+4, and *i*+7), whereas scaffolds **5**[16] and **6**[17,18] do not. Figure 1b presents an example by which the *i* side chain of **5a** is not the pseudo-C_α−C_β bond but pharmacophore mimetics.[16] Similarly, the *i*+4 side chains of **6** are not pseudo-C_α−C_β bonds.[17,18]

Double-facial mimetics such as **7**,[19] **8**,[20] and **9**[21] have also been developed as mimics of the LXXLL motif. Multifacial mimetics **10**[22] and **11**[23,24] have also been reported, although they are β-turn mimetics (Figure 2b).[22−24] Different stereoisomers of the cyclopropane scaffold of **11** were synthesized to mimic various conformations of peptidomimetics.

We also developed the multifacial α-helix mimetic compound **12a**,[25] designated as mS-11, which has the octahydropyrazino-[2,1-*c*]-1,2,4-oxadiazine scaffold **12**. The scaffold can mimic all four side chains involved in a one-turn helix. Compound **12a** is designed to inhibit binding of an intrinsically disordered protein NRSF/REST[26,27] to a receptor protein mSin3[28] by mimicking the one-turn α-helix motif, Leu46-Ile47-Met48-Leu49 (LIML), of the NRSF/REST. Compound **12a** is confirmed to interact with mSin3, inhibiting mSin3-NRSF/REST binding by NMR analysis (PDB ID: 5Y95).[25] It also ameliorates social interaction deficits in a prenatal valproic acid-induced autism mouse model.[29] Detailed in silico analysis by enhanced molecular dynamics simulation revealed that this scaffold induced PPI inhibition by long-range molecular orientation ordering followed by short-range interactions.[30]

Although many structural peptidomimetics have been developed, no analytical or validation method has been established to demonstrate quantitatively how similarly these molecules can mimic target peptide structures. This report describes two novel methods for analyzing structural peptidomimetics. They enable quantitative and visual understanding of the structural similarity of peptidomimetics to their target peptides based on comparison of side-chain C_α−C_β bonds and pseudo-C_α−C_β bonds.

RESULTS AND DISCUSSION

PCD Plot: Alignment-Free Method Based on C_α−C_β Bonds. For the analysis of protein structures such as secondary structures, Ramachandran plots[31] based on φ and ψ angles have often been used as a well-known powerful method. Comprehensive analysis of φ and ψ angle distribution in the Ramachandran plot has been reported for classification by secondary structure types and amino acid types using non-redundant protein structure sets.[32] The φ and ψ angle analysis is effective for analyzing peptide backbone structures, but it cannot be applied to structural peptidomimetics. The main chain is replaced completely by a small-molecule scaffold in structural peptidomimetics. Therefore, φ and ψ angles cannot be defined. This point of inadequacy might make it difficult to evaluate the similarity of structural peptidomimetics qualitatively with its target peptide motif.

Using another structural analysis approach, Garland et al.[33] demonstrated the utility of C_α−C_β bond vectors for the classification and analysis of β-turn structures. Grabowski et al.[34] developed a virtual screening technique that represents a molecular scaffold by its side-chain attachment points (exit vectors) and properties of the side-chain substituents. They applied it for identification of β-turn mimetics and HMG-CoA inhibitors. Shuto et al.[23,24] introduced principal component analysis (PCA) for the quantification of the three-dimensional (3D) structural diversity of mimetics in the chemical space and evaluated their stereoisomeric cyclopropane scaffolds in comparison with conformations of natural tetrapeptide motifs in an X-ray structure database. These studies demonstrate the utility of analytical elements for the structural analysis of peptide fragments in proteins.

https://doi.org/10.1021/acsomega.1c03967
ACS Omega 2021, 6, 26601−26612

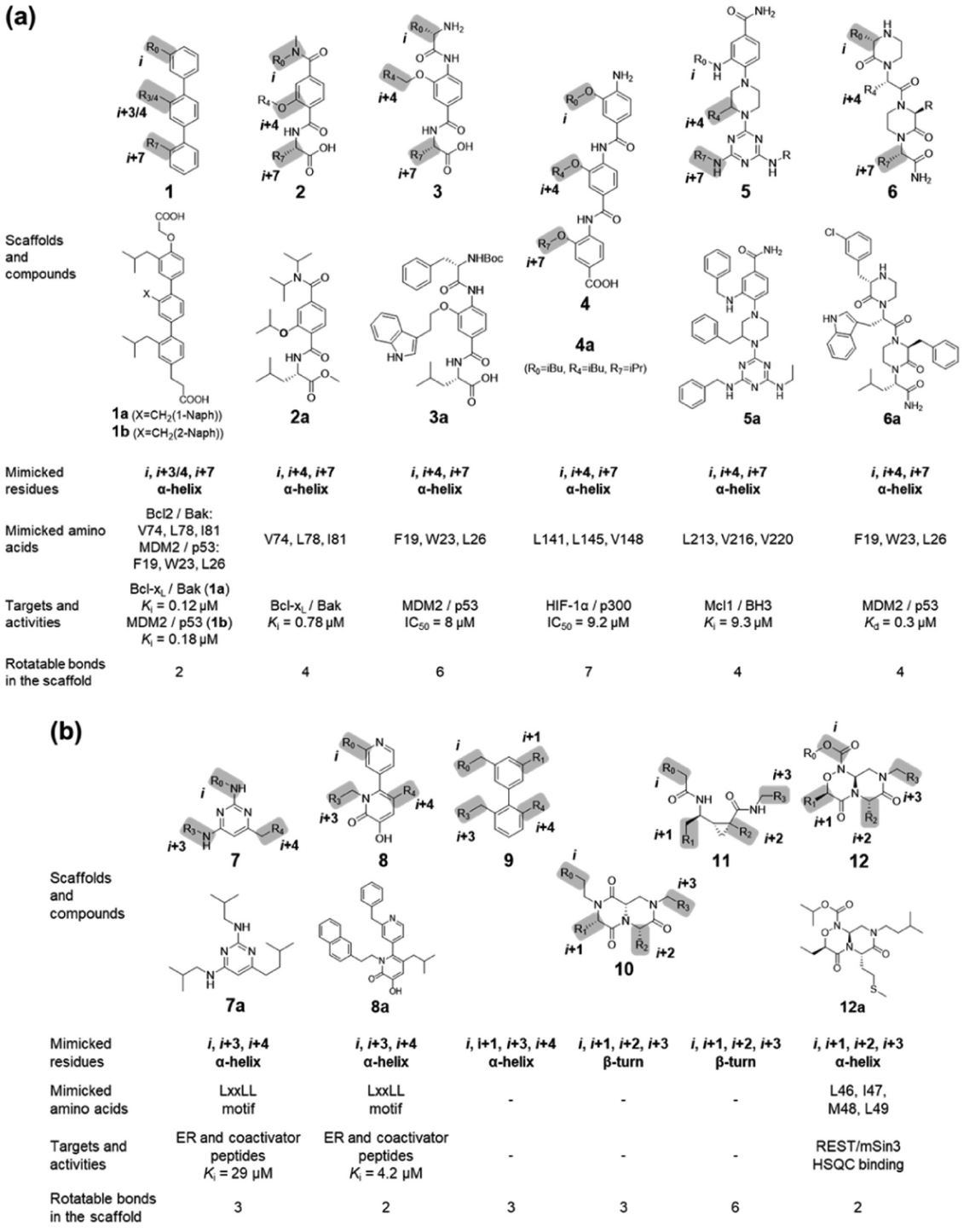

Figure 2. Lists of structural peptidomimetics (a) single-facial mimetics and (b) double-facial and multifacial mimetics. Chemical structures, mimetic amino acids/motifs, target proteins and activities, the number of rotatable bonds involved in the scaffolds, and references are shown. Substituents highlighted in gray are "pseudo-C_α−C_β bonds", which are designed to project side-chain C_α−C_β bonds. The pseudo-C_α−C_β bonds in these structural mimetics were assigned according to the description in the references. The *i* substituent of **5** and the *i* + 4 substituent of **6** are not pseudo-C_α−C_β bonds but pharmacophore mimetics (Figure 1 and its legend present the details). The rotational bonds are counted in the scaffolds inside the pseudo-C_α−C_β bonds.

Results of those earlier studies indicate the necessity of establishing a new method for visual and comprehensive evaluation of the conformations of the peptide fragments and peptidomimetics in the chemical space. Therefore, we attempted principal component analysis based on C_α−C_β bond vectors combined with the alignment-free shape comparison method and ultrafast shape recognition (USR) encoding.[35]

Figure 3a presents calculation methods and the workflow for PCD-plot[0123]. Details of the procedures are described in Method 1 and Figure S1. Figure 4 presents the results of distribution of conformations of the extracted peptide fragments constituted by *i*, *i*+1, *i*+2, and *i*+3 amino acid residues from

https://doi.org/10.1021/acsomega.1c03967
ACS Omega 2021, 6, 26601−26612

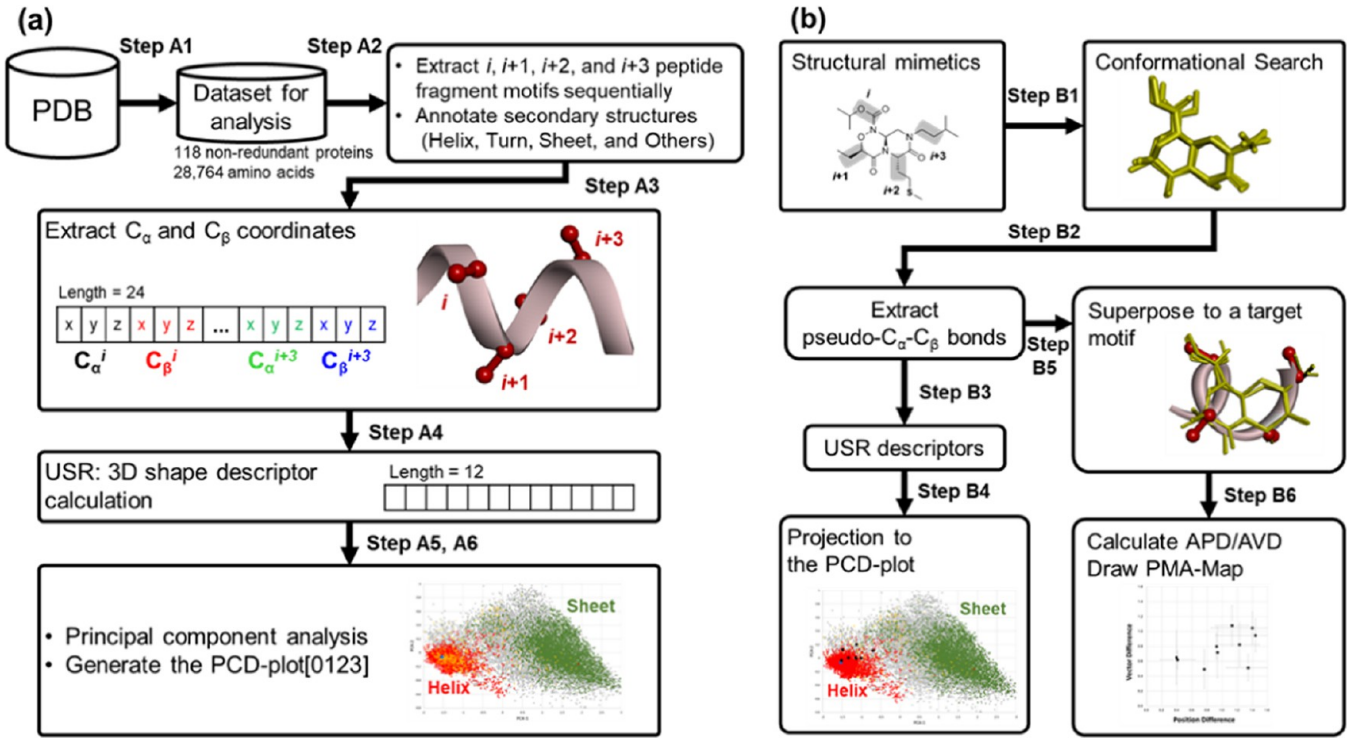

Figure 3. (a) Calculation workflow for PCD-plot[0123]. (b) Calculation workflow on the analysis of mimetic compounds: conformation generation, projection to the PCD plot, and illustration of the PMA map.

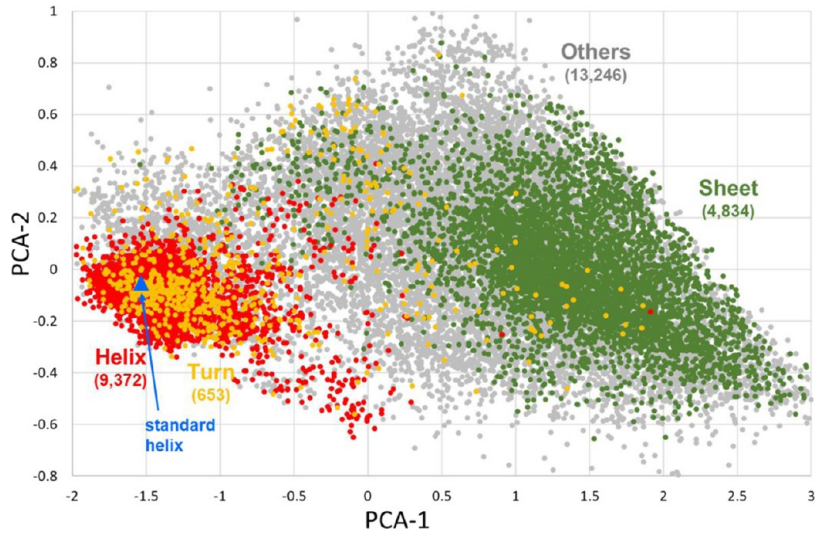

Figure 4. PCD-plot[0123]: principal component analysis map of conformational distribution on the peptide fragments extracted from nonredundant 118 proteins (Method 1). The continuous "*i*, *i*+1, *i*+2, and *i*+3" side chains were used for analysis. Each dot represents a peptide fragment. Helix (red), Turn (orange), Sheet (green), Others (gray), and the standard α-helix (blue triangle). Numbers in parentheses are numbers of shown data.

nonredundant sets of 118 proteins. The 28,105 extracted peptide fragment data set includes diverse structures such as the helix, sheet, turn, disordered, and random conformations and is appropriate for constructing the PCD plot, the chemical space of bond vectors. We designated this map as a peptide conformation distribution plot: PCD-plot[0123]. Numbers in square bracket notation represent the source of the side-chain number. Secondary structures were annotated for extracted peptide fragment motifs as the "Helix", "Sheet", "Turn" and "Others". Also, USR encoding was used to represent a shape formed by the set of $C_\alpha - C_\beta$ bond vectors extracted from a peptide fragment as a vector of 12 shape descriptors. Because USR is independent of the absolute coordinate system, molecular shapes can be compared directly without superposing the molecules. For this reason, the PCD plot is alignment free.

Figure 4 clarifies in a PCD plot that Helix (red), Turn (orange), and Sheet (green) form a cluster. The 9,372 Helix data gather on the left-side narrow area. The standard α-helix (blue triangle) is located at the Helix center, indicating that the description of the α-helix in the PCD plot is consistent with that in the Ramachandran plot because the standard helix is defined as a highly populated α-helix area by φ and ψ angles.[32] Consequently, the PCD plot can analyze peptide secondary structures effectively in the chemical space and can distinguish

https://doi.org/10.1021/acsomega.1c03967
ACS Omega 2021, 6, 26601−26612

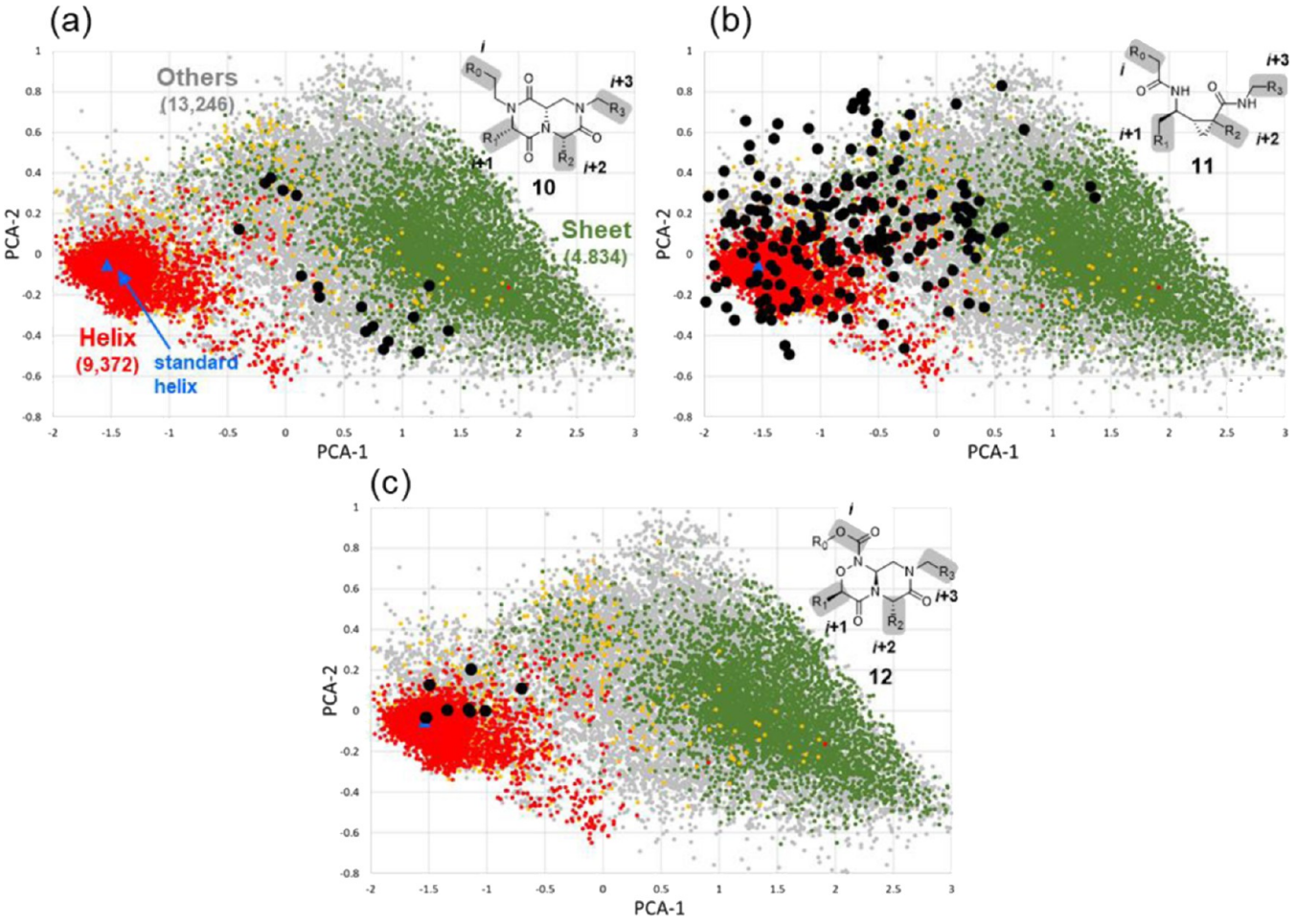

Figure 5. PCD-plot[0123] with the projection of multifacial peptidomimetic scaffolds **10** (a), **11** (b), and **12** (c). Each conformer is represented by a black dot. The Turn layer (orange) is sent to the back for clarification. The Other notation is the same as that shown in Figure 3.

secondary structures of peptide fragments using coordinates of C_α and C_β atoms, instead of φ and ψ angles in a Ramachandran plot. Several examples of structures demonstrate that a partially distorted and unwound α-helix is positioned at the edge of or outside of the Helix region (Figure S2). Distribution of the Turn is overlapped with the Helix. In actuality, the conformations of $C_\alpha-C_\beta$ bonds in the type I β-turn closely resemble those in the α-helix, except for the vector of the i+3 side chain (Figure S3).

Next, the multifacial mimetic scaffolds **10**−**12** were projected. They have i, i+1, i+2, and i+3 pseudo-$C_\alpha-C_\beta$ bonds on PCD-plot[0123] (Figure 5). Calculation workflows are presented in Figure 3b and Method 2. Calculation examples are shown in Figure S4. This analysis, an alignment-free method, uses conformations of peptidomimetics projected to the PCD plot representing the chemical space of peptide fragments. Multiple conformations were assessed for each molecule using conformational search calculations. Accordingly, we can clarify the distribution of conformations of mimetic compounds and can also avoid arbitrary selection of a specified conformation suitable for the superposition. Black dots in Figure 5 denote each conformation of a scaffold. Conformations of **10** are located on the central region of the map. They are distributed widely because of high flexibility of the i side chain (Figure 5a). Conformations of **11** are spread out quite broadly, including the Helix region (Figure 5b) because **11** has six rotatable bonds in the scaffold and has high conformational flexibility. In this case, large entropic costs are concerned in the binding of the target protein. The conformation distribution of **12** is located on the limited area within the Helix region (Figure 5c), indicating **12** as a superior scaffold for multifacial α-helix mimetics.

The single-facial mimetics **1**−**4** were also projected on PCD-plot[047]. They have i, i+4, and i+7 pseudo-$C_\alpha-C_\beta$ bonds (Figure 6a−d). To analyze a different set of pseudo-$C_\alpha-C_\beta$ bonds, a separate PCD plot must be prepared for the corresponding $C_\alpha-C_\beta$ bond sets. The calculation method is the same as that shown in Figure 4, where sets of the i, i+4, and i +7 side chains are extracted for analysis instead of the i, i+1, i+2, and i+3 sets in PCD-plot[0123]. The resulting maps and the meaning of the PCA-1 axis showed a similar tendency to that of PCD-plot[0123] (Table S3). The conformations of **1** and **2** are gathered in a small area. They are located near the left side of the Helix region, whereas those of **3** are located onto the Helix area. Conformations of **4** (with seven rotatable bonds) are spread broadly, but some parts are distributed within the Helix region. Scaffolds **5** and **6** cannot be projected on a PCD plot because some side chains are not pseudo-$C_\alpha-C_\beta$ bonds but are pharmacophore mimetics (Figure 1b). Double-facial mimetics **7**−**9** having i, i+3, and i+4 pseudo-$C_\alpha-C_\beta$ bonds were also projected on PCD-plot[034] (Figure 6e−g). Distributions of all mimetics are located on the limited area within or near the Helix region, indicating that these scaffolds are good α-helix mimetics.

In summary, the PCD plot is an alignment-free analysis based on the $C_\alpha-C_\beta$ atom coordinates. It enables visual and comprehensive understanding of the conformations of peptide

https://doi.org/10.1021/acsomega.1c03967
ACS Omega 2021, 6, 26601−26612

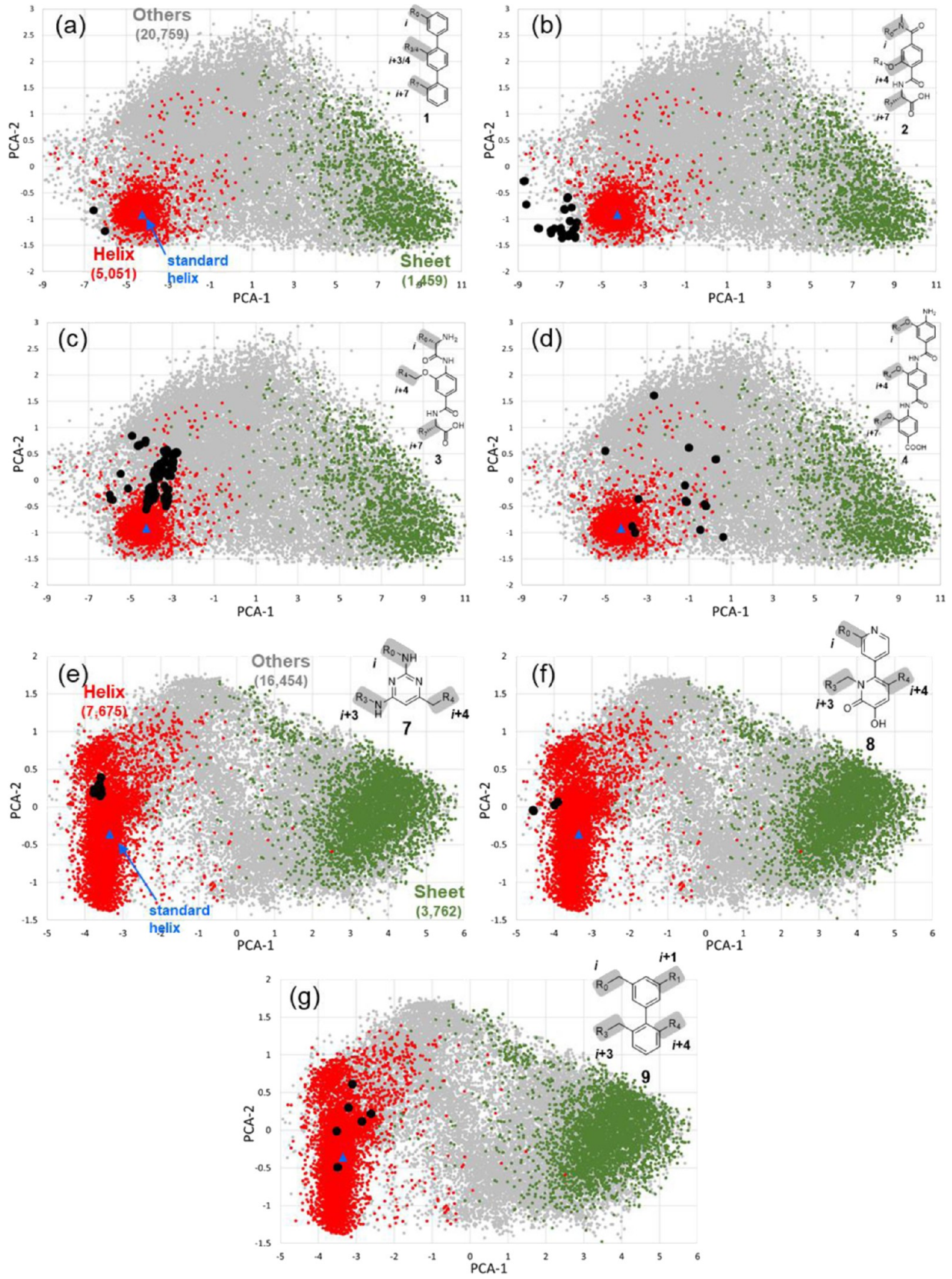

Figure 6. (a−d) PCD-plot[047]: PCA analysis using the *i*, *i*+4, and *i*+7 side chains and projection of single-facial mimetic compounds **1**−**4**. (e−g) PCD-plot[034]: PCA analysis using *i*, *i*+3, and *i*+4 side chains and projection of double-facial mimetic compounds **7**−**9**. Notations are the same as those used in Figure 3.

fragments and classification of secondary structures likely by the Ramachandran plot but based on an alternative concept. Projection of a peptidomimetic molecule to the PCD plot visually clarifies the position of their conformation distribution

https://doi.org/10.1021/acsomega.1c03967
ACS Omega 2021, 6, 26601−26612

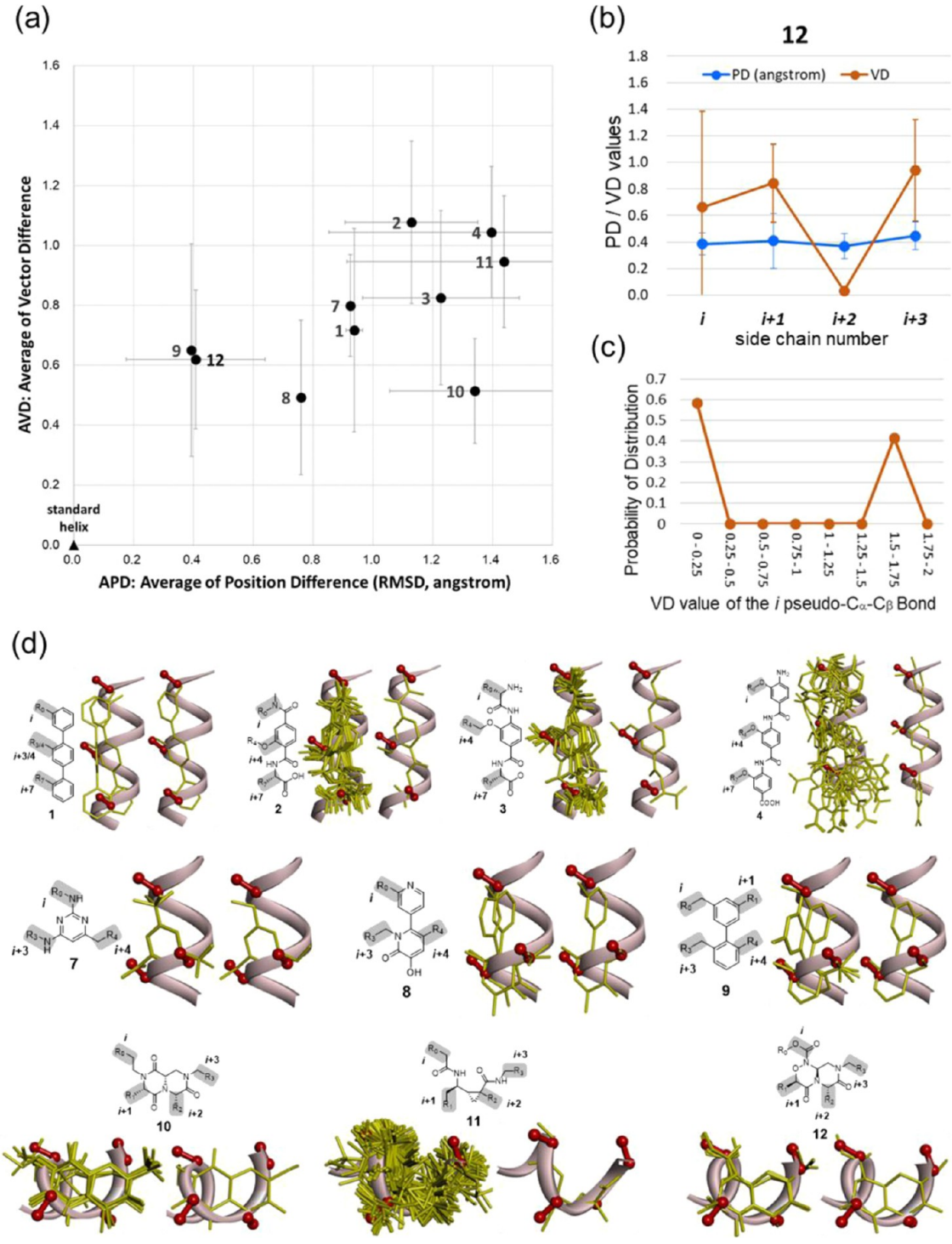

Figure 7. (a) Helix mimetics analyzer (HMA) map. The *x*-axis and *y*-axis, respectively, denote the average of position difference (APD, Å) and the average of vector difference (AVD). Error bars show the standard deviation. (b) Detailed helix mimetic analysis of **12** for each pseudo-C_α−C_β bond. (c) Orientational distribution of the *i* pseudo-C_α−C_β bond of **12**. (d) Superposed views with α-helix and mimetic compounds. Yellow and red denote each conformer and C_α−C_β bond, respectively. Chemical structures, all conformers (left), and a representative conformer for clarification (right).

and how widely their conformations spread on the chemical space of peptide fragments. It also reveals the three-dimensional structural similarity of mimetics to its target peptide and protein secondary structures. Peptidomimetic analysis using the PCD plot showed that mimetic scaffolds **7**, **8**, **9**, and **12** are excellent α-helix mimetics.

PMA Map: Alignment Method Based on C_α−C_β Bonds. Projection of structural peptidomimetics on the PCD plot facilitates our understanding of their conformational features visually in the chemical space. However, from the prospective of drug design and scaffold selection, it is important to ascertain how precisely, in detail and quantitatively, the molecules can mimic a specified target motif. We therefore developed the peptidomimetic analysis map (PMA map), shown in Figure 7a. The calculation workflow is presented in Figure 3b. Detailed procedures are described in Method 3 and Figure S5. This

https://doi.org/10.1021/acsomega.1c03967
ACS Omega 2021, 6, 26601−26612

analysis is regarded as an alignment-based method because it is based on the structural superposition of a peptidomimetics and its target peptide motif. In this map, the *x*-axis is the average of position difference (APD), the root-mean-square deviation (RMSD, Å) between C_α atoms in a peptide motif and the corresponding atoms in a mimetic molecule. The *y*-axis is the average of vector difference (AVD), where the difference of orientation between a $C_\alpha-C_\beta$ bond vector and its pseudo-$C_\alpha-C_\beta$ bond vector is represented as "1−inner product of the two vectors". When a standard α-helix is set to a reference motif, we designate it the helix mimetic analysis map (HMA map). Different from the PCD plot, the PMA map is independent of the choice of the set of side chains. In other words, we can compare peptidomimetics with different sets of pseudo-$C_\alpha-C_\beta$ bonds, such as **1** and **12**, on the same PMA map and can compare them directly.

Figure 7a clearly presents quantified analysis results of the structural mimetics shown in Figure 2. Scaffolds **9** and **12** have APD values of less than 0.5 Å in the map, meaning that the positions of the C_α-corresponding atoms in scaffolds **9** and **12** are closer to those of C_α atoms of the standard α-helix than those of others. The AVD values of scaffolds **9** and **12** are around 0.6, which means that the directions of their pseudo-$C_\alpha-C_\beta$ bond vectors show better agreement with those of $C_\alpha-C_\beta$ bond vectors of a standard α-helix than those of other mimetic scaffolds. The two scaffolds also showed good results on the PCD plot, as described above. Scaffolds **1**, **2**, **3**, **4**, **10**, and **11** are more deviated from the standard α-helix in the HMA map, which are consistent with the distribution location in their PCD plot. Error bars of **4** and **11** in the map are large, which also accords with their wide distribution on the PCD plot and the crowded superposing view (Figure 7d). The HMA map shows conformity with the α-helix structure, with similarity between the $C_\alpha-C_\beta$ bonds of the α-helix and their pseudo-$C_\alpha-C_\beta$ bonds, which differs among mimetic scaffolds. The results are consistent with those of the PCD plot for most of the evaluated peptidomimetic scaffolds.

Detailed analyses of pseudo-$C_\alpha-C_\beta$ bonds were performed with scaffold **12** (Figure 7b) and other scaffolds (Figure S6). In scaffold **12**, the PD values of all pseudo-$C_\alpha-C_\beta$ bonds are around 0.4 and good superposition with the four C_α atoms. The *i*+2 VD value is 0.03 ± 0.03, which means that the *i*+2 pseudo-$C_\alpha-C_\beta$ bond mimics the *i*+2 moiety of the standard α-helix almost completely. The *i*+1 VD value is 0.84 ± 0.29 and large, which is derived from the fact that the stereochemistry of the carbon atom at the 3-position of **12** is reverse to that of the natural amino acid. The *i* and *i*+3 VD values are, respectively, 0.66 ± 0.72 and 0.94 ± 0.38. These large deviations are attributable to the flip-flop of the carbamate group for the *i* VD value (Figure 7c) and existence of a free rotatable bond for the *i* +3 VD value. These analyses of **12** revealed that the positions of the C_α-corresponding atoms are close to those of the four C_α atoms of the α-helix and revealed that the mimetics has flexibility in the direction of its pseudo-$C_\alpha-C_\beta$ bonds. Although this point can also be confirmed visually from superposed views (Figure 7d), quantitative analysis of each pseudo-$C_\alpha-C_\beta$ bond explicitly shows characteristics such as the position, direction, flexibility, and sophistication of mimicking, which can guide the development or improvement of new mimetic scaffolds.

The PMA map, an alignment-based analysis, uses $C_\alpha-C_\beta$ bonds and pseudo-$C_\alpha-C_\beta$ bonds. It can evaluate the similarity of a mimetic compound with its target peptide motif in chemical space by quantified parameters. It incorporates consideration of the conformation and flexibility of the mimetic molecules. Moreover, it is useful to compare three-dimensional structures of different peptidomimetics having different sets of pseudo-$C_\alpha-C_\beta$ bonds. The HMA map clarified that scaffolds **9** and **12** are α-helix mimetics superior to others.

Detailed Analysis of the PCD Plot. Here, we discuss the usefulness of the PCD plot based on the meanings of axes. Coefficients of the PCA-1 and PCA-2 axes are presented in Table S3. Moment-1 and moment-2 of fct and ftf of PCA-1 showed large coefficients in PCD-plot[0123], suggesting that PCA-1 roughly represents the molecular size. The coefficients of PCA-1 in PCD-plot[047] and PCD-plot[034] have similar characters. For example, scaffold **1** is projected on the left side of the Helix region (Figure 6a). The meaning of PCA-1 implies that the molecule is smaller than the α-helix. In actuality, a superposing view of the α-helix and **1** shows that **1** is shorter than the α-helix (Figure 7d). It is interesting that the alignment-based analysis and alignment-free analysis point out the same feature, but differently. The meanings of the PCA-2 axis differ among PCD plots; they are complicated. Specific examination of PCD-plot[0123] reveals that moment-3 occupies the major component, which represents the molecule asymmetry and skewness. Conformations on the lower area of the map show a symmetric shape, whereas those in the upper area have symmetry-breaking structures (Figure S7).

Regarding PCD-plot[0123], α-helix structures (shrink form regularly arranged by hydrogen bonds) are located on the left side of the map, whereas β-turn structures (extended form regularly arranged by hydrogen bonds) are located on the right side. In these areas, the distribution range on the PCA-2 axis is limited. In contrast, random structures (gray dots) range mainly on the middle region of the PCA-1 axis but spread widely along the PCA-2 axis. This result is consistent with the fact that various structures are included, such as symmetric and distorted conformations without hydrogen bond constraints. Therefore, the resulting chemical spaces in PCD-plot[0123] form a triangle.

The ratio of the explained variance of the PCA-1 is greater than 0.9. In the case of PCD-plot[0123], the 24 coordinate components extracted from four $C_\alpha-C_\beta$ bonds of peptide fragments are ultimately reduced to two axes using principal component analysis. Alternatively, the relative positions of the four $C_\alpha-C_\beta$ bonds can be expressed by eight φ and ψ angles. Moreover, the angles are not independent. As presented in the Ramachandran plot, the angles are limited in a specified set and are mutually related. Therefore, the chemical space of $C_\alpha-C_\beta$ bond sets might be expressed intrinsically using a small set of independent variants. The PCD plot expresses the chemical space by $C_\alpha-C_\beta$ bonds of peptide fragment motifs. The Ramachandran plot indicates peptide secondary structures by φ and ψ angles of each amino acid residue in peptides. Consequently, the PCD plot can be a useful and visible method for representing protein structures and peptidomimetics in a chemical space, similar to the Ramachandran plot, however, based on different analytical viewpoints.

Comparison of the PCD Plot and PMA Map. Table 1 presents the PCD plot and PMA map features. Both methods are based on analysis of $C_\alpha-C_\beta$ bonds and pseudo-$C_\alpha-C_\beta$ bonds, not φ and ψ angles, in which multiple conformations for mimetic molecules are considered. The PCD plot, an alignment-free method, can visualize the three-dimensional structure of peptide fragments comprehensively. Projection of a mimetic molecule clarifies its conformation distribution in the chemical space and

https://doi.org/10.1021/acsomega.1c03967
ACS Omega 2021, 6, 26601−26612

Table 1. Feature Summary of the PCD Plot and the PMA Map

features	PCD plot	PMA map
input data	$C_\alpha-C_\beta$ bonds and pseudo-$C_\alpha-C_\beta$ bonds	
conformation of mimetics	multiple conformations considered	
molecular alignment	alignment free	alignment-based
position on the chemical space of peptide fragments	visualized	–
similarity evaluation of mimetics against the target motif	comparison of plot position	quantified evaluation by APD and AVD
distribution of conformers	each conformer visualized	only average and standard deviation
analysis of each pseudo-$C_\alpha-C_\beta$ bond	difficult	possible
comparison of mimetics with different pseudo-$C_\alpha-C_\beta$ bond sets	separate map necessary	possible on the same map

similarity with its target peptide secondary structures. We can infer that a molecule with a widespread conformational distribution would require entropic costs in binding to its target protein. It is noteworthy that the PCD plot can express even a deviated distribution of conformations because each dot represents a single conformation. We prepared PCD-plot[0123], PCD-plot[047], and PCD-plot[034], where a separate map must be used to compare mimetic molecules with different sets of pseudo-$C_\alpha-C_\beta$ bonds.

The PMA map, in contrast, is an alignment-based method. Unlike the PCD plot, a single PMA map can compare various peptidomimetics with different sets of pseudo-$C_\alpha-C_\beta$ bonds. The map can evaluate the similarity between an arbitrary target motif and its mimetic molecules using APD and AVD values. Unlike the PCD plot, this analysis provides detailed similarity evaluation based on each pseudo-$C_\alpha-C_\beta$ bond. Elucidating the actual conformational distribution is difficult because it is integrated into average and standard deviation values. The whole chemical space formed by peptide fragments cannot be described in this map. Consequently, these two methods have distinctive characteristics and complementary roles. Both results can provide us features of peptidomimetic molecules from different perspectives. They are expected to be useful for the rational design and development of new scaffolds suitable for an individual PPI target.

CONCLUSIONS

We developed two novel methods, the PCD plot and PMA map, for visualized and quantified evaluation of peptidomimetics. These methods analyzed three-dimensional structures of peptide fragments and peptidomimetics based on $C_\alpha-C_\beta$ bonds, instead of φ and ψ angles in the traditional Ramachandran plot. It is important that conformation distributions of the molecules be considered when using these two new methods. The PCD plot enables visual and comprehensive analyses of the conformations of peptide fragments and the classification of protein secondary structures, similar to the Ramachandran plot, by specifically addressing multiple pseudo-$C_\alpha-C_\beta$ bonds. The projection of structural peptidomimetics on the PCD plot reveals its position and distribution of conformations in the chemical space, with similarity to its target peptide motif as an indicator. PMA map gives quantified similarity indices between peptidomimetics. It compares structures of different peptidomimetics having different sets of pseudo-$C_\alpha-C_\beta$ bonds, which support analysis and evaluation of the similarity of peptidomimetics based on features of the respective pseudo-$C_\alpha-C_\beta$ bonds. The two methods clarified that **9** and our scaffold **12** are α-helix mimetics superior to others examined for this study. These results demonstrate that the two methods are complementarily useful for rational PPI drug discovery. Consequently, by applying these methods, we are now developing new peptidomimetic scaffolds, conducting PPI drug discovery, and constructing a compound library targeting PPIs, a subject that will be described in a future publication.

METHODS

Preparation of Nonredundant Protein Data Sets and the PCD Plot. Workflows are shown in Figure 3a. Detailed procedures and examples for PCD-plot[0123] and PCD-plot[034] are presented in Figure S1.

Step A1. Preparation of nonredundant protein data sets. The selection method is based on a description presented in the literature.[32] From conditions on X-ray diffraction to a resolution of 2.0 Å or higher, the number of distinct protein entities = 1, the sequence length >100, human proteins, and registration after the year 2000, we selected 7,178 protein structures from the Protein Data Bank (PDB) as on 27 August 2020. From the selected proteins, we extracted 200 proteins randomly and removed redundant proteins by manual inspection. The final sets of selected structures were 118 nonredundant proteins containing 28,764 amino acids (List S1). The DSSP secondary structure types[36,37] were assigned for each amino acid. The number of the respective DSSP secondary structure types is listed in Table S1.

Step A2. Extraction of peptide fragments. To make PCD-plot[0123], the "*i*, *i*+1, *i*+2, and *i*+3" peptide fragment motifs were extracted from the head to the tail with one amino acid shift from the selected 118 proteins. The number of extracted motifs was 28,105. Examples of fragments 1−5 from PDB_ID:1gf0 are shown in Figure S1. Secondary structures "Helix", "Sheet", "Turn", and "Others", were annotated for each motif. When the DSSP types of four amino acids have three or four continuous G/H/I, T, and E, the motifs are defined, respectively, as Helix, Turn, and Sheet. The remaining types were assigned to Others. For PCD-plot[047] and PCD-plot[034], the "*i*, *i*+4, and *i*+7" and the "*i*, *i*+3, and *i*+4" motifs were extracted, respectively. Secondary structures were annotated similarly. In these two motifs, Turn is not defined because the β-turn structure is constructed by four continuous amino acids. Table S2 lists the number of annotated secondary structures for the extracted motifs (peptide fragments).

Step A3. Extraction of the C_α and C_β atom coordinates from each fragment. The *XYZ* coordinates of "*i*, *i*+1, *i*+2, and *i*+3" C_α and C_β atoms are extracted for PCD-plot[0123]; the *XYZ* coordinates of "*i*, *i*+3, and *i*+4" C_α and C_β atoms are extracted for PCD-plot[034]. Examples are shown in Figure S1.

Step A4. Conversion to ultrafast shape recognition (USR) descriptors. The extracted coordinate sets were converted to a vector of 12 shape descriptors using USR encoding,[35] which is calculated from the distribution of the interatomic distance derived from a set of four reference points. As an alignment-free shape comparison method, USR has been used in virtual screening against arylamine N-acetyltransferases.[38] The 12 descriptors used for calculations consist of four molecular locations and three moments. The four molecular locations are the molecular centroid (ctd), the closest atom to ctd (cst), the farthest atom from ctd (fct), and the farthest atom from fct (ftf). As the three moments, the first moment is the average atomic distance to the molecular centroid (an estimate of the molecular size). The second is the square root of the variance of these

https://doi.org/10.1021/acsomega.1c03967
ACS Omega 2021, 6, 26601−26612

atomic distances about the first moment. The third moment is the skewness of these atomic distances about the first moment (i.e., a measure of the asymmetry of the distribution). We used the skewness instead of the cubic root of the skewness used in the original report from the literature[35] because we balanced the descriptors to make a better classification of secondary structures of peptide fragment motifs. The balances of the roots are also discussed in that original report.[35]

Steps A5 and A6. Dimension reduction was conducted using principal component analysis (PCA) to generate a PCD plot. The first and second components (PCA-1 and PCA-2) were assigned to *x*- and *y*-axes for 2D graph representation. The PCA calculations were performed using Scikit-learn (https://jmlr.csail.mit.edu/papers/v12/pedregosa11a.html).

Conformation Generation of Peptidomimetics and Its Projection to the PCD Plot. Figure 3b portrays a workflow for the conformational search of peptidomimetics and its projection to the PCD plot. Details of the procedures and examples of scaffold **12** are displayed in Figure S4 for clarification.

Step B1. Conformational search of peptidomimetics. Conformations of mimetic molecules were generated using the "Conformer Distribution" function of computational chemistry software Spartan'18 ver. 1.4.4 (Wavefunction Inc.). The calculations were conducted using the MMFF force field and "SEARCHMETHOD = MONTECARLO, FINDBOATS" options, which can explore a wide conformation space including the flip-flop of scaffold rings. All side chains in mimetic molecules are modeled to a methyl group (corresponding to the alanine side chain) to avoid unsuccessful side-chain conformation searching. Considering the coarse-grained calculation level, all generated conformers within 10 kcal/mol from the most stable conformation were adopted for analyses.

The free rotatable bonds in the peptidomimetic molecules presented in Figure 2 are few (2−7). Therefore, most of the possible conformational space can be covered by the conformational search using Spartan software. Hehre et al. report the validity of conformational ensemble using Spartan based on agreement of NMR chemical shifts calculated from the generated conformers with the experimental data.[39] Importantly, PCD plot and PMA map results on peptidomimetic molecules depend on the obtained conformational ensemble. Therefore, in the analysis of larger and more flexible peptidomimetic molecules, another conformational search method such as multicanonical MD might be appropriate.

Step B2. Generated conformations were exported to sdf files. The *XYZ* coordinate sets of pseudo-C_α−C_β bonds were extracted from each conformer. For scaffold **12**, the coordinates of "*i*, *i*+1, *i*+2, and *i*+3" pseudo-C_α and C_β atoms are extracted (Figure S4). This step corresponds to step A3.

Step B3. The 24 extracted coordinate data sets were converted to a vector of 12 shape descriptors, as described in step A4.

Step B4. The PCA-1 and PCA-2 values were calculated using the PCA coefficients (Table S3) found in step A5. They are projected to the PCD plot.

Superposition with Standard α-Helix and PMA Map Generation. Figure 3b presents a workflow for the procedures (steps B5 and B6). Details of the procedures and examples of scaffold **12** are shown in Figure S5.

Steps B1 and B2 are the same as those in Method 2.

Step B5. Superposition to a target motif. C_α atoms (pseudo-C_α atoms) in pseudo-C_α−C_β bonds of a mimetic molecule were superimposed onto the corresponding C_α atoms of a target motif using the rdAlignment module implemented in RDKit: Open-source cheminformatics software (https://www.rdkit.org/). In mimetic scaffold **12**, four pseudo-C_α atoms were superposed onto the four C_α atoms in a standard α-helix. The standard α-helix was generated using the poly-Ala sequence with $\psi = -63.8°$ and $\varphi = -41.1°$, which is known as the highly populated area of the actual α-helix in the PDB.[32]

Step B6. Calculation of position and vector differences and projection to the PMA map. The position difference (PD, Å) is defined as the Euclidean distance between the pseudo-C_α atom of a molecule and the corresponding C_α atoms of a target motif. The APD is defined as RMSD between the pseudo-C_α atoms of a mimetic molecule and the corresponding C_α atoms of a target motif. In addition, after the superposition, the vector difference (VD) is calculated as

$$\mathrm{VD} = 1 - \langle \mathbf{v}_{\alpha\beta}^{P}, \mathbf{v}_{\alpha\beta}^{M} \rangle$$

where $\mathbf{v}_{\alpha\beta}{}^{P}$ is a unit vector from the C_α coordinate to the C_β coordinate of a target motif, $\mathbf{v}_{\alpha\beta}{}^{M}$ is a unit vector from the C_α coordinate to the C_β coordinate of the pseudo-C_α−C_β bond in a mimetic molecule, and the inner product is denoted by <−,−>. In this formulation, each of the unit vectors was translated so that its starting point (C_α coordinate) was at the origin. The average value of VD for every conformation is defined as AVD. The VD value is normalized. It ranges from 0 to 2. The APD/AVD values and their standard deviations used for the PMA map were calculated from every conformer and every pseudo-C_α−C_β bond in a mimetic molecule.

■ ASSOCIATED CONTENT

Supporting Information

The Supporting Information is available free of charge at https://pubs.acs.org/doi/10.1021/acsomega.1c03967.

PDB ID of 118 nonredundant proteins used for analyses; detailed procedures and examples for the PCD plot; assignment of DSSP secondary structure types; secondary structure annotation for extracted peptide fragment motifs; coefficients of PCA axes; examples of peptide motif structures in the PCD plot; superposed views of the α-helix and β-turn; detailed procedures and examples for mapping conformations to the PCD plot; detailed procedures and examples for superposition and PMA-map generation; detailed helix mimetic analysis of mimetic scaffolds **1**−**11**; and examples of peptide fragment conformers (PDF)

■ AUTHOR INFORMATION

Corresponding Author

Hajime Takashima − *Research and Development Department, PRISM BioLab Co., Ltd., Fujisawa, Kanagawa 251-0012, Japan*; orcid.org/0000-0002-7436-040X; Phone: +81-466-25-2555; Email: takashima@prismbiolab.com

Authors

Atsushi Yoshimori − *Chemoinformatics & AI Research Group, Institute for Theoretical Medicine, Inc., Fujisawa, Kanagawa 251-0012, Japan*

Eiji Honda − *Research and Development Department, PRISM BioLab Co., Ltd., Fujisawa, Kanagawa 251-0012, Japan*

Tomonori Taguri − *Research and Development Department, PRISM BioLab Co., Ltd., Fujisawa, Kanagawa 251-0012, Japan*

https://doi.org/10.1021/acsomega.1c03967
ACS Omega 2021, 6, 26601−26612

Jun Ozawa − *Research and Development Department, PRISM BioLab Co., Ltd., Fujisawa, Kanagawa 251-0012, Japan*
Masaji Kasai − *Research and Development Department, PRISM BioLab Co., Ltd., Fujisawa, Kanagawa 251-0012, Japan*
Satoshi Shuto − *Faculty of Pharmaceutical Science, Hokkaido University, Sapporo, Hokkaido 060-0812, Japan;* orcid.org/0000-0001-7850-8064
Dai Takehara − *Research and Development Department, PRISM BioLab Co., Ltd., Fujisawa, Kanagawa 251-0012, Japan*

Complete contact information is available at: https://pubs.acs.org/10.1021/acsomega.1c03967

Author Contributions

H.T. and A.Y. conceived and designed the research. H.T., A.Y., E.H., T.T., J.O., and D.T. performed the research. H.T. and A.Y. wrote the article. E.H. and M.K. revised the article. S.S. proposed the name of the pseudo-C_α−C_β bond and revised the article. D.T. supervised the research. All authors have given approval to the final version of the manuscript.

Notes

The authors declare no competing financial interest.

■ ACKNOWLEDGMENTS

The authors thank Dr. Hiroyuki Kouji for contributions on the prototype of the PMA map.

■ ABBREVIATIONS

APD, average of position difference; AVD, average of vector difference; HMA, helix mimetic analysis; NRSF/REST, neuron-restrictive silencer factor/RE1-silencing transcription factor; PCA, principal component analysis; PCD, peptide conformation distribution; PD, position difference; PDB, Protein Data Bank; PMA, peptidomimetic analysis; PPIs, protein−protein interactions; RMSD, root-mean-square deviation; USR, ultrafast shape recognition; VD, vector difference

■ REFERENCES

(1) Conte, L. L.; Chothia, C.; Janin, J. The Atomic Structure of Protein-Protein Recognition Sites. *J. Mol. Biol.* **1999**, *285*, 2177−2198.
(2) Guharoy, M.; Chakrabarti, P. Secondary Structure Based Analysis and Classification of Biological Interfaces: Identification of Binding Motifs in Protein-Protein Interactions. *Bioinformatics* **2007**, *23*, 1909−1918.
(3) Sawyer, N.; Watkins, A. M.; Arora, P. S. Protein Domain Mimics as Modulators of Protein−Protein Interactions. *Acc. Chem. Res.* **2017**, *50*, 1313−1322.
(4) Milroy, L. G.; Grossmann, T. N.; Sven, H.; Luc, B.; Christian, O. Modulators of Protein- Protein Interactions. *Chem. Rev.* **2014**, *114*, 4695−4748.
(5) Bullock, B. N.; Jochim, A. L.; Arora, P. S. Assessing Helical Protein Interfaces for Inhibitor Design. *J. Am. Chem. Soc.* **2011**, *133*, 14220−14223.
(6) Pelay-Gimeno, M.; Glas, A.; Koch, O.; Grossmann, T. N. Structure-Based Design of Inhibitors of Protein-Protein Interactions: Mimicking Peptide Binding Epitopes. *Angew. Chem., Int. Ed.* **2015**, *54*, 8896−8927.
(7) Watkins, A. M.; Bonneau, R.; Arora, P. S. Side-Chain Conformational Preferences Govern Protein-Protein Interactions. *J. Am. Chem. Soc.* **2016**, *138*, 10386−10389.
(8) Davis, J. M.; Tsou, L. K.; Hamilton, A. D. Synthetic Non-Peptide Mimetics of α-Helices. *Chem. Soc. Rev.* **2007**, *36*, 326−334.
(9) Jayatunga, M. K. P.; Thompson, S.; Hamilton, A. D. α-Helix Mimetics: Outwards and Upwards. *Bioorg. Med. Chem. Lett.* **2014**, *24*, 717−724.
(10) Wilson, A. J. Helix Mimetics: Recent Developments. *Prog. Biophys. Mol. Biol.* **2015**, *119*, 33−40.
(11) Yin, H.; Lee, G. I.; Hyung, S. P.; Payne, G. A.; Rodriguez, J. M.; Sebti, S. M.; Hamilton, A. D. Terphenyl-Based Helical Mimetics That Disrupt the P53/HDM2 Interaction. *Angew. Chem., Int. Ed.* **2005**, *44*, 2704−2707.
(12) Kutzki, O.; Park, H. S.; Ernst, J. T.; Orner, B. P.; Yin, H.; Hamilton, A. D. Development of a Potent Bcl-XL Antagonist Based on α-Helix Mimicry. *J. Am. Chem. Soc.* **2002**, *124*, 11838−11839.
(13) Yin, H.; Lee, G. I.; Sedey, K. A.; Rodriguez, J. M.; Wang, H. G.; Sebti, S. M.; Hamilton, A. D. Terephthalamide Derivatives as Mimetics of Helical Peptides: Disruption of the Bcl-XL/Bak Interaction. *J. Am. Chem. Soc.* **2005**, *127*, 5463−5468.
(14) Shaginian, A.; Whitby, L. R.; Hong, S.; Hwang, I.; Farooqi, B.; Searcey, M.; Chen, J.; Vogt, P. K.; Boger, D. L. Design, Synthesis, and Evaluation of an a-Helix Mimetic Library Targeting Protein-Protein Interactions. *J. Am. Chem. Soc.* **2009**, *131*, 5564−5572.
(15) Burslem, G. M.; Kyle, H. F.; Breeze, A. L.; Edwards, T. A.; Nelson, A.; Warriner, S. L.; Wilson, A. J. Small-Molecule Proteomimetic Inhibitors of the HIF-1α-P300 Protein-Protein Interaction. *ChemBioChem* **2014**, *15*, 1083−1087.
(16) Moon, H.; Lee, W. S.; Oh, M.; Lee, H.; Lee, J. H.; Im, W.; Lim, H. S. Design, Solid-Phase Synthesis, and Evaluation of a Phenyl-Piperazine-Triazine Scaffold as α-Helix Mimetics. *ACS Comb. Sci.* **2014**, *16*, 695−701.
(17) Tošovská, P.; Arora, P. S. Oligooxopiperazines as Nonpeptidic α-Helix Mimetics. *Org. Lett.* **2010**, *12*, 1588−1591.
(18) Lao, B. B.; Drew, K.; Guarracino, D. A.; Brewer, T. F.; Heindel, D. W.; Bonneau, R.; Arora, P. S. Rational Design of Topographical Helix Mimics as Potent Inhibitors of Protein-Protein Interactions. *J. Am. Chem. Soc.* **2014**, *136*, 7877−7888.
(19) Rodriguez, A. L.; Tamrazi, A.; Collins, M. L.; Katzenellenbogen, J. A. Design, Synthesis, and in Vitro Biological Evaluation of Small Molecule Inhibitors of Estrogen Receptor α Coactivator Binding. *J. Med. Chem.* **2004**, *47*, 600−611.
(20) Becerril, J.; Hamilton, A. D. Helix Mimetics as Inhibitors of the Interaction of the Estrogen Receptor with Coactivator Peptides. *Angew. Chem., Int. Ed.* **2007**, *46*, 4471−4473.
(21) Jacoby, E. Biphenyls as Potential Mimetics of Protein α-Helix. *Bioorg. Med. Chem. Lett.* **2002**, *12*, 891−893.
(22) Golebiowski, A.; Klopfenstein, S. R.; Chen, J. J.; Shao, X. Solid Supported High-Throughput Organic Synthesis of Peptide β-Turn Mimetics via Petasis Reaction/Diketopiperazine Formation. *Tetrahedron Lett.* **2000**, *41*, 4841−4844.
(23) Mizuno, A.; Kameda, T.; Kuwahara, T.; Endoh, H.; Ito, Y.; Yamada, S.; Hasegawa, K.; Yamano, A.; Watanabe, M.; Arisawa, M.; Shuto, S. Cyclopropane-Based Peptidomimetics Mimicking Wide-Ranging Secondary Structures of Peptides: Conformational Analysis and Their Use in Rational Ligand Optimization. *Chem. − Eur. J.* **2017**, *23*, 3159−3168.
(24) Mizuno, A.; Matsui, K.; Shuto, S. From Peptides to Peptidomimetics: A Strategy Based on the Structural Features of Cyclopropane. *Chem. − Eur. J.* **2017**, *23*, 14394−14409.
(25) Ueda, H.; Kurita, J.; Neyama, H.; Hirao, Y.; Kouji, H.; Mishina, T.; Kasai, M.; Nakano, H.; Yoshimori, A.; Nishimura, Y. A Mimetic of the MSin3-Binding Helix of NRSF/REST Ameliorates Abnormal Pain Behavior in Chronic Pain Models. *Bioorg. Med. Chem. Lett.* **2017**, *27*, 4705−4709.
(26) Schoenherr, C. J.; Anderson, D. J. The Neuron-Restrictive Silencer Factor (NRSF): A Coordinate Repressor of Multiple Neuron-Specific Genes. *Science* **1995**, *267*, 1360−1363.
(27) Chong, J. A.; Tapia-Ramirez, J.; Kim, S.; Toledo-Aral, J. J.; Zheng, Y.; Boutros, M. C.; Altshuller, Y. M.; Frohman, M. A.; Kraner, S. D.; Mandel, G. REST: A Mammalian Silencer Protein That Restricts Sodium Channel Gene Expression to Neurons. *Cell* **1995**, *80*, 949−957.

(28) Nomura, M.; Uda-Tochio, H.; Murai, K.; Mori, N.; Nishimura, Y. The Neural Repressor NRSF/REST Binds the PAH1 Domain of the Sin3 Corepressor by Using Its Distinct Short Hydrophobic Helix. *J. Mol. Biol.* **2005**, *354*, 903−915.
(29) Kawase, H.; Ago, Y.; Naito, M.; Higuchi, M.; Hara, Y.; Hasebe, S.; Tsukada, S.; Kasai, A.; Nakazawa, T.; Mishina, T.; Kouji, H.; Takuma, K.; Hashimoto, H. MS-11, a Mimetic of the MSin3-Binding Helix in NRSF, Ameliorates Social Interaction Deficits in a Prenatal Valproic Acid-Induced Autism Mouse Model. *Pharmacol. Biochem. Behav.* **2019**, *176*, 1−5.
(30) Higo, J.; Takashima, H.; Fukunishi, Y.; Yoshimori, A. Generalized-Ensemble Method Study: A Helix-Mimetic Compound Inhibits Protein-Protein Interaction by Long-Range and Short-Range Intermolecular Interactions. *J. Comput. Chem.* **2021**, *42*, 956−969.
(31) Ramachandran, G. N.; Sasisekharan, V. Conformation of Polypeptides and Proteins. *Adv. Protein Chem.* **1968**, *23*, 283−437.
(32) Hovmöller, S.; Zhou, T.; Ohlson, T. Conformations of Amino Acids in Proteins. *Acta Crystallogr., Sect. D: Biol. Crystallogr.* **2002**, *58*, 768−776.
(33) Garland, S. L.; Dean, P. M. Design Criteria for Molecular Mimics of Fragments of the β-Turn. 2. Cα-Cβ Bond Vector Analysis. *J. Comput.-Aided. Mol. Des.* **1999**, *13*, 485−498.
(34) Grabowski, K.; Proschak, E.; Baringhaus, K.; Rau, O.; Schubert-Xsilavecs, M.; Schneider, G. Bioisosteric Replacement of Molecular Scaffolds: From Natural Products to Synthetic Compounds. *Nat. Prod. Commun.* **2008**, *3*, 1355−1360.
(35) Ballester, P. J.; Finn, P. W.; Richards, W. G. Ultrafast Shape Recognition: Evaluating a New Ligand-Based Virtual Screening Technology. *J. Mol. Graphics Model.* **2009**, *27*, 836−845.
(36) Kabsch, W.; Sander, C. Dictionary of Protein Secondary Structure: Pattern Recognition of Hydrogen-Bonded and Geometrical Features. *Biopolymers* **1983**, *22*, 2577−2637.
(37) Touw, W. G.; Baakman, C.; Black, J.; Te Beek, T. A. H.; Krieger, E.; Joosten, R. P.; Vriend, G. A Series of PDB-Related Databanks for Everyday Needs. *Nucleic Acids Res.* **2015**, *43*, D364−D368.
(38) Ballester, P. J.; Westwood, I.; Laurieri, N.; Sim, E.; Richards, W. G. Prospective Virtual Screening with Ultrafast Shape Recognition: The Identification of Novel Inhibitors of Arylamine N-Acetyltransferases. *J. R. Soc. Interface* **2010**, *7*, 335−342.
(39) Hehre, W.; Klunzinger, P.; Deppmeier, B.; Driessen, A.; Uchida, N.; Hashimoto, M.; Fukushi, E.; Takata, Y. Efficient Protocol for Accurately Calculating ^{13}C Chemical Shifts of Conformationally Flexible Natural Products: Scope, Assessment, and Limitations. *J. Nat. Prod.* **2019**, *82*, 2299−2306.

https://doi.org/10.1021/acsomega.1c03967
ACS Omega 2021, 6, 26601−26612